IEICE TRANS. COMMUN., VOL. E76-B, NO. 11 NOVEMBER 1993

PAPER

Power Line Radiation over Eastern Asia Observed by the Satellite OHZORA

Ichiro TOMIZAWA† *and* Takeo YOSHINO†, *Members*

SUMMARY Statistically improved results of power line radiation (PLR) over Eastern Asia observed at 50 and 60 Hz are described in this paper. A total number of 150 orbits, which had been observed from June 1984 to January 1986, by the Japanese scientific satellite OHZORA, are used to detect PLR over Eastern Asia around the Japanese Islands. Depending on the increase in the number of data points, the statistical characteristics of the background noise can be precisely determined by using the improved technique compared with the initial analysis. Statistically reasonable data points are detected as PLR based on the $+3\sigma$ criterion, where σ is the standard deviation of the background noise. Therefore, the statistical reliability for rejecting the background noise is 99.85%. Then, these detected data are applied to the cause-and-effect test. When the statistically detected data points are placed on the map of Eastern Asia, the points cover Eastern Japan and the east coast of China for 50 Hz, and they cover Western Japan for 60 Hz. The maps of the detection ratios and those of the average field strengths indicate the positive correlation with the ground maps of the electric power generation at 50 and 60 Hz. The positive correlation is more clearly seen at 50 Hz since the background noise is somewhat weaker than that at 60 Hz. This close relationship between the satellite observation and the electric power generation suggests that the detection of PLR is not caused by chance, and that PLR penetrates into the ionosphere and propagates approximately just upward. The decrease of field strength with altitude can be interpreted as the gradual decrease of the refractive index from 400 to 700 km. Therefore, the detection ratio and the average field strength with respect to the satellite altitude suggest PLR propagating from the bottom of the ionosphere. According to these observational results, it is concluded that PLR in Eastern Asia is high above the high electric power generating regions over Japan and China, and that the satellite observation is capable of estimating PLR field below the ionosphere. These results are the first direct indication that the PLR field is enhanced over the high electric power generation region, and is penetrating into the ionosphere.

key words: *power line radiation, power line, Eastern Asia, ELF, satellite*

1. Introduction

Energy loss of electric power lines at the fundamental frequencies, 50 or 60 Hz, due to induction or radiation of electromagnetic fields is usually ignored as a small part in the total energy loss transmitting through power lines. Even though the loss is so small, the fields can be detected at distant places from power lines [9], [15] since the propagation loss at these frequencies is approximately 1 dB/1000 km for the propagation mode [5]. However, it is impossible to describe the real distribution maps of PLR over the wide regions from the remote observations because the mixing of the radiation fields of many sources limits the discrimination of each source. As the induced fields steeply attenuated at the source region [5], total electromagnetic fields radiated and induced from the power lines should be observed close to the source regions to reveal a horizontal map of the field strength of PLR over a large region. Therefore, the PLR fields should be surveyed at high altitudes close to or over the source region where power lines are extended, because the electromagnetic fields can be considered to represent not a local network of power lines but a wide one above this altitude [11]. The observation technique using balloons is normally limited to surveying a relatively small region because flights are only possible under the control of local safety agencies. On the other hand, we tried to observe an upward propagation of PLR fields using scientific rockets in the ionosphere [15]. From those observations, we found out that a small part of PLR can penetrate into the ionosphere. Therefore, this satellite observation was planned to survey a large region where power lines are extended [10].

Electric power generation in Eastern Asia is concentrated in the industrial regions, especially in Japan and the People's Republic of China (hereafter abbreviated to China) [13]. Moreover, these regions are characterized by two different generation frequencies, 50 and 60 Hz. The frequency of 50 Hz is used in Eastern Japan, China, the Democratic People's Republic of Korea (hereafter abbreviated to North Korea) and the Union of Soviet Socialist Republics (hereafter abbreviated to USSR). The frequency of 60 Hz is used in Western Japan, the Republic of Korea (hereafter abbreviated to South Korea), Taiwan, and the Republic of the Philippines (hereafter abbreviated to Philippines). It is interesting to note that Japan, whose electric generation is the largest in this region [13], is divided into two regions according to the power generation frequency [4], and that a large region of sea where no power lines are extended is placed in the southeastern half of the observation region [10].

Manuscript received January 29, 1993.
Manuscript revised April 21, 1993.

† The authors are with the Faculty of Electro-Communications, The University of Electro-Communications, Chofu-shi, 182 Japan.

Thus this distribution of electric power systems in Eastern Asia can be considered as a high-contrast region for the study of PLR.

Based on our observation of the magnetic field at 50 and 60 Hz using the satellite OHZORA in the topside of the ionosphere in 1984, we have shown some results detecting the power line radiation in our last paper [10]. It was revealed that the detection of PLR is not easy since the PLR field strength is not so high compared to that of the background noise. Therefore we introduced a statistical detection method on the $+1\sigma$ criterion without compensating the skewness of the distribution since the total number of the observation data was limited to 31 orbits through this period. As we mentioned in Paper (10), data points which exceeded the $+1\sigma$ criterion did not randomly scatter over the observation region. The correlation between the electric power generation in China and the distribution of the detected data points at the east coast of China was agreeable. Therefore, we could clearly show the correlation if we adopted a more stringent criterion.

In this paper, we are going to illustrate the distribution maps of PLR in Eastern Asia for the first time as the major result of our study. To improve the statistical reliability of PLR detection, a procedure to estimate the statistical characteristics of the background noise is developed using an iterative calculation to reduce the contamination of PLR to the estimation of the background noise parameters. This iterative calculation can be done since a large number of orbits are used for analysis at this time. Accordingly the detection criterion is to be statistically explained based on the difference in the amplitude distribution. Then, we test these detected data as to whether they correlate with the ground distribution of the electric power generation in Eastern Asia or not, because the cause-and-effect relationship between the source and the radiated field must be clearly revealed. Finally, we will discuss the altitude dependencies and distribution maps of the detected data to explain the propagation of PLR into the ionosphere.

2. Improvement of the Method of Detecting PLR

2. 1 Interpretation of the Influence of PLR on the Observation Data

An expected scheme of the influence of PLR on the observation data is described in Fig. 1. According to Paper (10), the background noise shows good correlation among the field strengths at 50, 55, and 60 Hz. If the statistical characteristic of the background noise is assumed to be a wideband Gaussian noise, the correlation diagram of the background noise at 50 or 60 Hz with that at 55 Hz should be scattered along the straight line as shown in the left panel. If PLR is superposed on some of this background noise, total magnetic fields at these points should be moved upward from the original positions as shown in the central panel. The degree of the shift depends on the ratio of PLR field to the background noise field. When

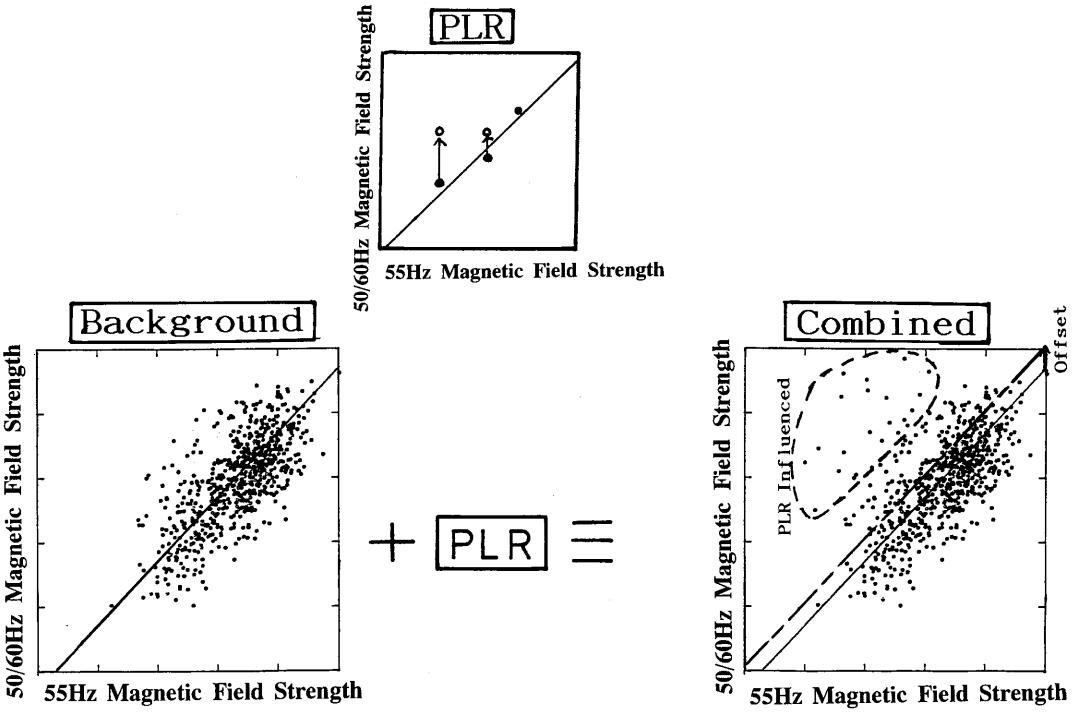

Fig. 1 Expected scheme of the influence of power line radiation (PLR) on background noise.

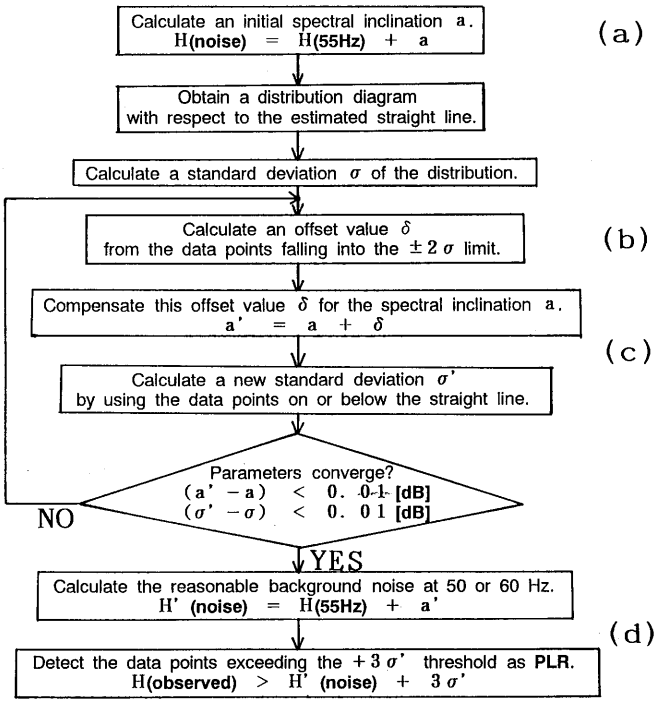

Fig. 2 Flow chart for estimating the real amplitude distribution of the background noise from the observation data which is disturbed by PLR. Steps of this estimation process are illustrated in Fig. 3.

these influenced data are combined with the normal background noise data, the resulting correlation diagram may be shifted relatively upward as shown in the right panel. In this case, the least-square-fitted line indicating the statistical mean of the distribution shifts upward, as indicated by the dashed line. This shift means that the amplitude distribution after combination is skewed. Therefore, the original statistical characteristic parameters of the background noise must be estimated under such a disturbed condition in order to clearly discriminate the PLR data from the observation data.

2.2 Improved Method of Estimating Statistical Parameters of the Background Noise

A flow chart for estimating the real amplitude distribution of the background noise from the observation data, which is disturbed by PLR, is shown in Fig. 2. The main purpose of this method is to obtain reasonable statistical parameters of the background noise, and to detect the data influenced by PLR as the statistically different characteristics. Steps of this estimation process are also described by a simulation process in Fig. 3.

First, we assume that the statistical parameters of observation data are close to the original ones when the observed fields at 50 or 60 Hz mainly consist of the background noise. This assumption has been

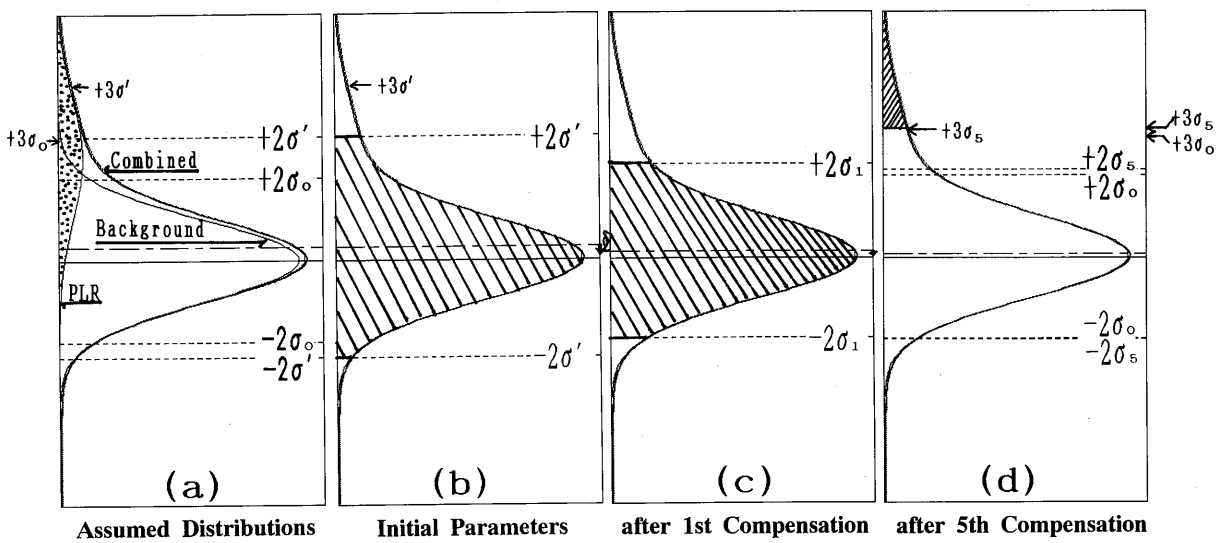

Fig. 3 The figures, (a)-(d), illustrate the steps of the process described in Fig. 2. The assumed distribution of observation data is "Combined" as the result of the summation of the "Background" noise and "PLR." The hatched area within the $\pm 2\sigma'$ limit in (b) is averaged to obtain the offset value $\boldsymbol{\delta}$. Compensating this offset value to $\boldsymbol{a}$, we can get the next spectral inclination value $\boldsymbol{a}'$. Then, calculating the standard deviation by limiting the data below this compensated line as indicated by the dashed line in (c), the new standard deviation $\boldsymbol{\sigma}_1$ is obtained. This recalculation process is repeated until convergence is achieved.

confirmed since the statistical analysis of the initial observation has shown a good agreement with the broadband Gaussian noise [10]. Second, based on this assumption, we calculate the first estimate of the statistical characteristics of the distribution as described in line (a) of the flowchart of Fig. 2, taking all of the observation data into consideration. These values must not be far from the real values of the background noise since the disturbance is believed to be weak. Third, we calculate the second estimate of the offset by limiting the number of data that must be within the $\pm 2\sigma$ limit as described in line (b) of the flowchart of Fig. 2, since this portion of data is less disturbed than all of the observation data. Fourth, after compensating the offset, we calculate the standard deviation by limiting the data that must be less than the compensated spectral inclination line as described in line (c) of the flowchart of Fig. 2, since the disturbance should also be weak for the lower half of the observed distribution. This estimation process is continued to give sufficiently good fitting parameters to a Gaussian distribution. Note that the obtained offset value corresponds to the spectral inclination of the background noise at these observation frequencies, as shown in Fig. 4 of Paper (10).

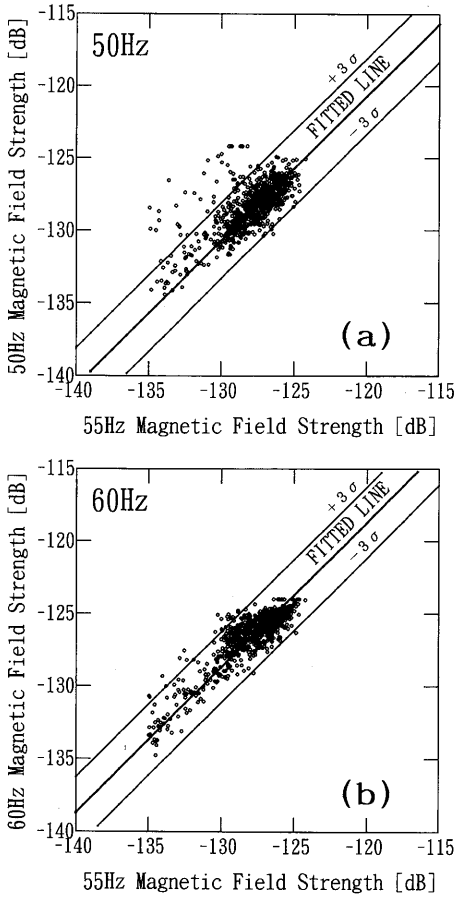

Fig. 4 (a) Correlation diagram between the field strength at 50 Hz and that at 55 Hz. (b) Correlation diagram between the field strength at 60 Hz and that at 55 Hz. The fitted line indicates the center of the distribution of the background noise, and the 3σ lines indicate the 3σ limits of the Gaussian distribution with respect to the fitted line. These characteristic parameters of these distributions are calculated by the process described in Fig. 2.

We will show an example of simulation of the estimation process described above to reveal its effectiveness. The steps of this estimation process proceed from Fig. 3(a) to Fig. 3(d), which correspond to the same characters in parenthesis indicated on the right side of Fig. 2. At first, we assume the distributions as follows: 1) the main background noise distribution has the zero mean value, $\boldsymbol{a}=0.0$, and the standard deviation, $\boldsymbol{\sigma}=\sigma_0$, where σ_0 is the standard deviation of the background noise, 2) the influenced field distribution is assumed as the mean value of $\boldsymbol{a}=+2.5\sigma_0$ and the standard deviation of $\boldsymbol{\sigma}=\sigma_0$ in order to emphasize the influence, and 3) the number ratio of the secondary distribution to the main distribution is 10%. This simulation method is used for estimating the real amplitude distribution with respect to the correlation line between the magnetic field strength at 50 or 60 Hz and the field strength at 55 Hz. Most of the observation data are filled with the background noise which has a Gaussian distribution as shown by the curve named "Background." Some part of the observation includes the contribution of PLR at 50 or 60 Hz. Since the contribution curve named "PLR" is not so much amount of data points, the integrated field strength at these frequencies slightly increases their amplitude relative to the background noise as shown by the curve named "Combined." Thus the distribution is scattered to the upper side where the observed strength is greater than the estimated strength. Therefore, the resulting distribution can be illustrated as the curve "Combined." Note that the curve "Combined" is somewhat deviated upward from the curve "Background," which indicates the main contribution of the background noise, especially at the lower half of the distribution. The combined distribution is again shown in Fig. 3(b) in hatching the region within the $\pm 2\sigma'$ limit. The data in this hatched region are averaged to obtain the offset value $\boldsymbol{\delta}$. Compensating this offset value to $\boldsymbol{a}$, we can get the next spectral inclination value $\boldsymbol{a}'$. Then, calculating the standard deviation by limiting the data below this compensated line as indicated by the dash-dotted line in Fig. 3(c), we get the new standard deviation $\boldsymbol{\sigma}_1$. This recalculation process is repeated in such a manner that $\boldsymbol{\sigma}$ and $\boldsymbol{\delta}$ are converged. After the 5th compensation when the process converges, the estimated values become $\boldsymbol{a}_5=+0.11\sigma_0$ and $\boldsymbol{\sigma}_5=1.03\sigma_0$. These values are approximately equal to the original values compared to the first estimation. Therefore the threshold to detect PLR can effectively represent the background noise characteristics.

Statistically estimated parameters, $\boldsymbol{a}'$ and $\boldsymbol{\sigma}'$, are applied to the next detection process as described in

line (d) of the flowchart of Fig. 2. As the possibility of exceeding the $+3\sigma$ limit of the background noise should be 0.0015, the portion exceeding the $+3\sigma$ limit is possibly uncorrelated with the background noise. Thus the exceeded portion can be attributed to PLR since PLR works by enhancing the magnetic field strength at 50 or 60 Hz, as shown in Fig. 1.

2. 3 Actual PLR Detection Process

The PLR observation was made over Eastern Asia using the equipment onboard the scientific satellite OHZORA, and the observed data were directly telemetered to the Kagoshima Space Center (KSC) of the Institute of Space and Astronautical Science (ISAS). The period of the observation data used in this process is from June 1984 to January 1986. The total number of orbits is 150, yielding five times as much the data as in Paper (10). As the data were limited to the real time observation due to the interference from the data recorder [10], the coverage of observation was from 110 to 160°E in longitude and from 5 to 55°N in latitude. The coverage area includes Eastern Asian countries such as Japan, China, South Korea, North Korea, Taiwan, Philippines and USSR, where two power generating frequencies are used and power generation is relatively concentrated to small regions. One data point represents an average magnetic field strength during 30 sec. The data interval of 30 sec was originally selected so as to match the satellite orbital data which were provided by ISAS. The 1361 data points remain after rejection of those that are disturbed or interfered with. Although shortening of the data interval is possible, the statistical fluctuation of the amplitude distribution such as Fig. 5 tends to be broader so that it can be difficult to detect the influence of PLR. Therefore, no more shortening is performed in this paper.

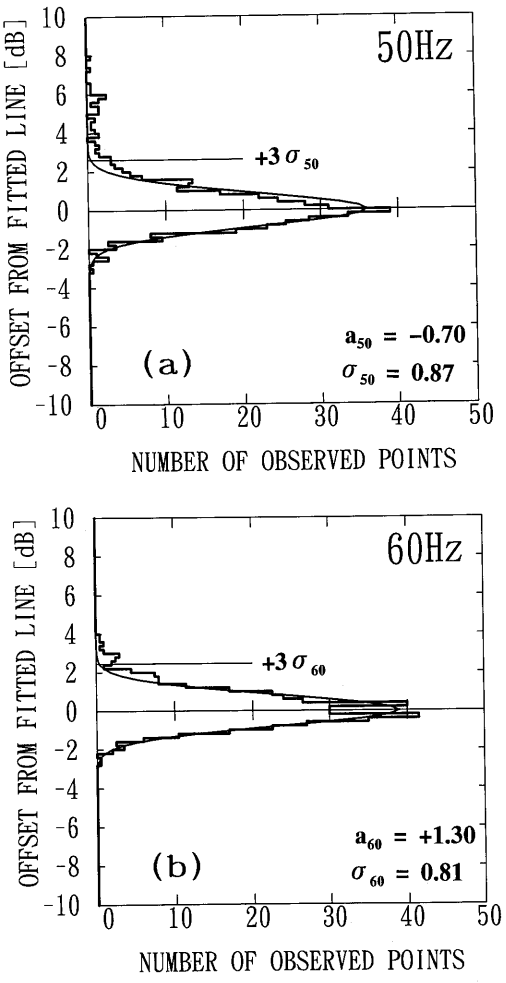

Fig. 5 Distribution, (a) for 50 Hz, and (b) for 60 Hz, with respect to the fitted line which is estimated by the process as indicated in Fig. 2. The actual distribution is indicated by the histogram with the 0.2 dB bin. The estimated Gaussian distribution curve is shown by the solid curve. The $+3\sigma$ limit is indicated by the thin line.

The diagram between the field strength at 50 Hz and that at 55 Hz is shown in Fig. 4(a). The similar one between the field strength at 60 Hz and that at 55 Hz is shown in Fig. 4(b). Note that the magnetic field strength is described in dB throughout this paper with respect to the unit magnetic field strength of 1 A/m. (The magnetic field strength of -120 dB, i.e., 10^{-6} A/m, can be converted to another useful unit of the magnetic field strength as 1.2 pT.) As the effective bandwidth of the PLR receivers is 1 Hz, the background noise field strength can also be interpreted as the unit of A/m·Hz$^{1/2}$. The fitted line indicates the center of the distribution of the background noise, and the 3σ lines indicate the 3σ limits of the normal distribution with respect to the fitted line. The characteristic parameters of these distributions are calculated by the process described in Fig. 2. The observation data points scatter out of the $+3\sigma$ limit for the upper distribution at both frequencies, while the 3σ limit for the lower distribution contains almost all of the data. This means that the scattering of the data points is caused by PLR as described in Fig. 1.

Distributions with respect to the fitted lines, which are estimated by the process as indicated in Fig. 2, are shown in Fig. 5(a) for the case of 50 Hz and in Fig. 5 (b) for the case of 60 Hz. The actual distribution is indicated by the histogram with the 0.2 dB bin. The estimated normal distribution is illustrated by the solid curve. The $+3\sigma$ limit is also indicated by the thin line. The estimated spectral offset $\boldsymbol{a}$ and the estimated standard deviation $\boldsymbol{\sigma}$ are also indicated in the same panel. As these estimated curves show good fit to the observed distributions, it is suggested that the observation data mainly contain the background noise with a little bit of or without the influence of PLR. Thus our first assumption of the disturbance rate of PLR to the background noise is confirmed by this result. Addi-

tionally the statistical characteristics are similar at both frequencies, since the standard deviations of these two distributions are similar in magnitude, i.e., 0.87 dB and 0.81 dB for 50 and 60 Hz, respectively. The corresponding values in Paper (10) were 1.09 dB and 0.98 dB for 50 and 60 Hz, respectively. The values of the current analysis are smaller than the previous ones, which indicates the effectiveness of this improved method of estimation. Therefore the second assumption of the wideband Gaussian noise can also be confirmed. The spectral inclination values are -0.7 dB/5 Hz for 50 Hz, and $+1.30$ dB/5 Hz for 60 Hz. The corresponding values in Paper (10) were -0.525 dB/5 Hz for 50 Hz, and $+1.25$ dB/5 Hz for 60 Hz. This value is quite different for 50 Hz, while it is approximately the same for 60 Hz.

It can be seen that some of the data points exceed the $+3\sigma$ limit on both panels of Figs. 4 and 5. These data points are considered as the PLR influenced data points in the detection process. The number of data exceeding the limit is larger for 50 Hz than for 60 Hz. The number of detected data points is 45 for 50 Hz and 21 for 60 Hz.

3. Distribution Maps of Detection Ratio and Average Magnetic Field Strength over Eastern Asia

3. 1 Mapping Procedure

As we mentioned before, this satellite observation covered Eastern Asian countries. These countries can be separated into two groups depending on the power generating frequencies, i.e. 50 or 60 Hz. The former includes Eastern Japan, China, North Korea, and USSR, and the latter includes Western Japan, South Korea, Taiwan and Philippines. Therefore, we conducted a cause-and-effect test for each frequency region. Mapping the observation data over Eastern Asia is performed with the unit of a $5^\circ \times 5^\circ$ square box since the number of the observed data and especially the number of the detected data becomes too small if we divide them into smaller square boxes.

The displaying format both for Fig. 6 and for Fig. 7 is as follows: (a) The number of observation points within the $5^\circ \times 5^\circ$ square is placed in each box on the map. (b) The percent detection ratios of each square are indicated only for the detected one with a shading scale indicated above. The average field strength in dB value is indicated in each square box in (c) for all of the observed points, and in (d) for the detected points. The higher field strength is shown in a darker shade, as the scale indicated. The two horizontal maps, (b) and (d), for the detected data points correlate with (e) the electric power generation of Eastern Asian countries in 1985 [13].

3. 2 Mapping the Distributions of the Observed and the Detected Data for 50 Hz

Horizontal mapping over Eastern Asia for 50 Hz is shown in Fig. 6. Note that the electric power generation of the far-eastern part of USSR is not indicated in Fig. 6(e), since it is impossible to separate the contribution of this region from the statistical data. Hence we do not mention the correlation of the detection with the contribution from the far-eastern part of USSR.

It is clearly seen from Fig. 6(b) that the detected locations of PLR at 50 Hz are concentrated in two regions: one is Eastern Japan and the other is the east coast of China. Although the number of observation points is relatively small over the eastern half of the map as seen in Fig. 6(a), a statistically sufficient number of points spread over most of the boxes. Therefore these high detection ratios over Eastern Japan in Fig. 6(b) must be real. As there is no concentration of the higher field regions as seen in Fig. 6(c), detected points should scatter all over the observation region for noncorrelating cases. Thus this correlation must be real. Additionally the enhancement of the field strength close to the Japanese Islands and to the east coast of China as seen in Fig. 6(d) strongly suggests a correlation with the high-power-generating regions, as indicated in Fig. 6(e) [4], [6], [13], [14].

3. 3 Mapping the Distributions of the Observed and the Detected Data for 60 Hz

Horizontal mapping over Eastern Asia for 60 Hz is shown in Fig. 7. The format of figures is the same as in Fig. 6 but the observation frequency is 60 Hz. Since the frequency of the electric power generation system in USSR is 50 Hz, we can fully correlate the detection with the ground map. Although the detected boxes are spread over a relatively large region compared to those for 50 Hz, they do spread around the 60 Hz regions: Western Japan, Taiwan, and Philippines. Additionally, the relatively higher detection ratios concentrate around Western Japan, where the electric power generation is the highest in Eastern Asia [4], [13]. As the relative enhancement of the observed field strength can also be neglected for 60 Hz, the concentration of the detected boxes due to the electric power generation of 60 Hz as shown in Fig. 7(e) should be real especially for Western Japan. It is, however, impossible to clearly correlate the detected boxes around Taiwan and Philippines with the electric power generations of these regions.

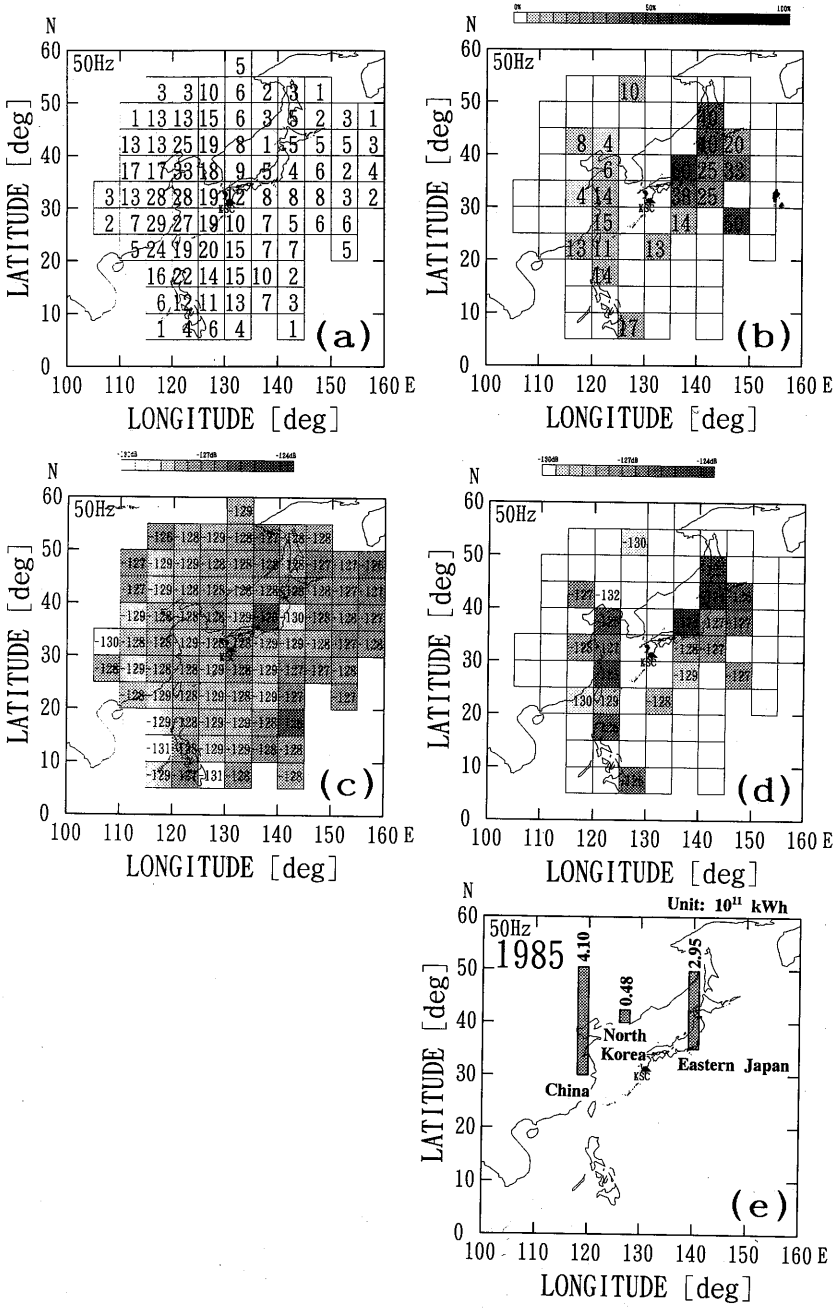

Fig. 6 (a) Horizontal distribution of all of the observation data points on the Eastern Asia map at 50 Hz. The number of observation points within the 5°×5° square is placed in each box on the map. (b) The percent detection ratios of each square box are shown only for the detected ones with a shading scale indicated above. (c) The average field strengths of all observation points. (d) The average field strength of the detected points in each square. The field strength is indicated in dB (0 dB=1 A/m). Higher field strength is shaded darker as indicated above. (e) The total electric power generation in Eastern Asia in 1985.

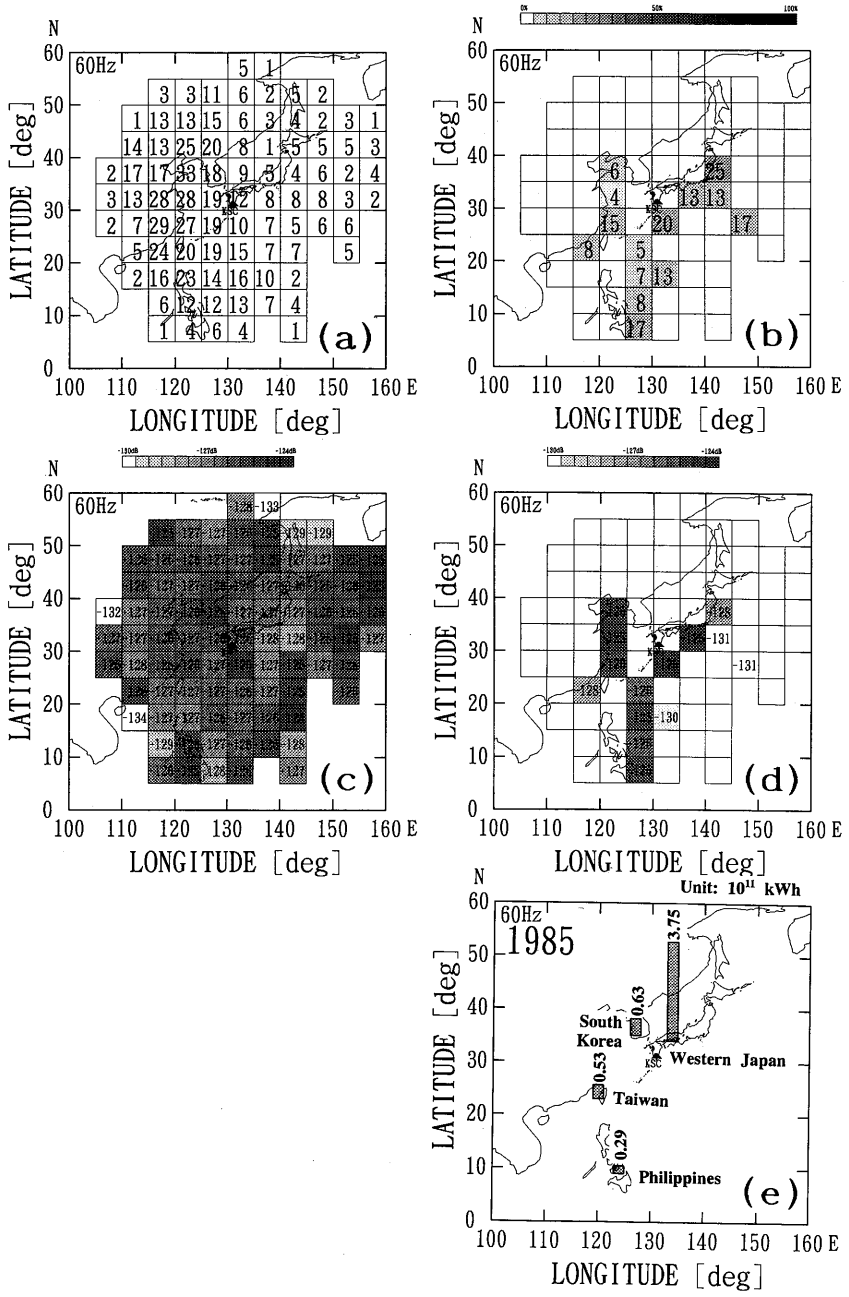

Fig. 7 The format of figures is the same as Fig. 6 but the observation frequency is 60 Hz.

4. Altitude Dependencies of the Detection Ratio and the Average Field Strength

4. 1 Altitude Dependency of the Detection Ratio

Altitude dependencies for 50 Hz are shown in Fig. 8 as follows: (a) the number of observation data points per unit altitude, (b) the number of detected data points per unit altitude, and (c) the detection ratio for each unit altitude. Altitude dependencies for 60 Hz are shown in Fig. 9 in the same format as Fig. 8.

The number of observed points is approximately 50 from 350 to 600 km, and becomes approximately 100 from 600 to 800 km, as shown in Fig. 8(a). It can be seen from this figure that all of the altitude bins contain at least 50 data points, and that there are no bins of statistically low reliability. However, the number of detected points is mainly distributed from 350 to 600 km. Therefore, the detection ratios for each altitude are strongly enhanced at the lower altitudes. The maximum detection ratio is 22% for 350 to 400 km. The detection ratio seems to gradually decrease with increasing altitude.

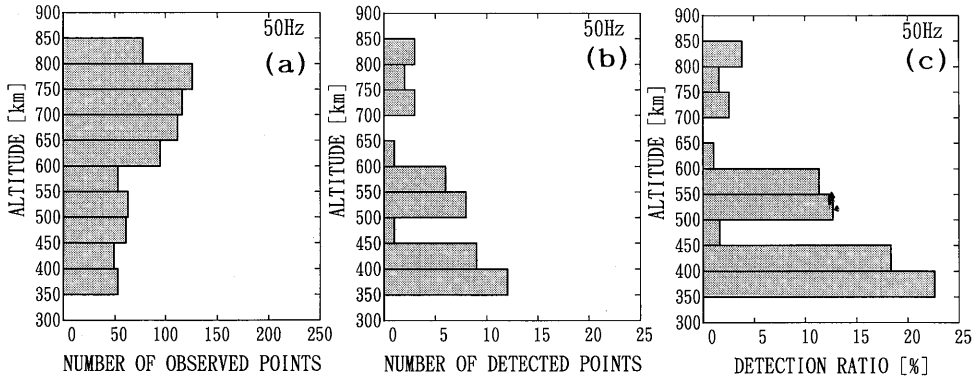

Fig. 8 Altitude dependency, (a) of all of the observed data points, (b) of the detected data points, and (c) of the detection ratio, for 50 Hz.

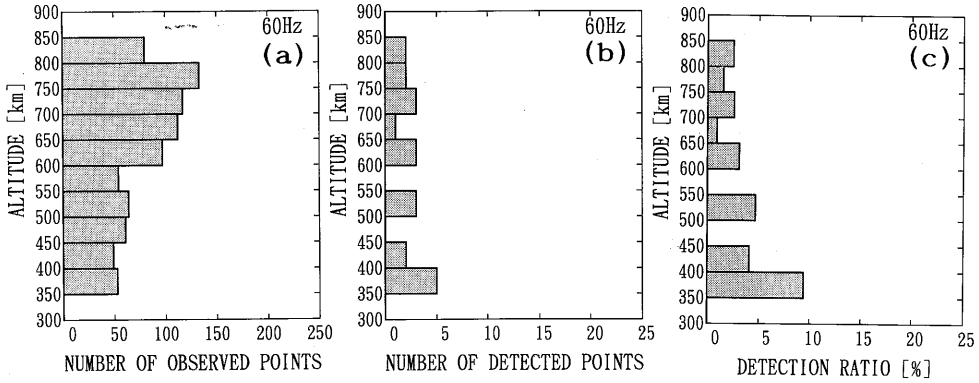

Fig. 9 Altitude dependency, (a) of all of the observed data points, (b) of the detected data points, and (c) of the detection ratio, for 60 Hz.

Although the number of observed points for 60 Hz is almost the same as that for 50 Hz, the number of detected points does not show strong enhancement at lower altitudes, as seen in Fig. 9(c). However, the total detection ratio at lower altitudes is slightly enhanced compared to the upper ones. The maximum detection ratio is 9% for 350 to 400 km, and the ratio seems also to decrease gradually with increasing altitude.

4.2 Altitude Dependencies of the Average Field Strength

Average magnetic field strength versus satellite altitude for 50 Hz is shown in Fig. 10(a) for all of the observed data points, and in Fig. 10(b) for the detected data points. The horizontal short lines across the top of each bar are the standard deviation of each field strength. Shaded bars in Fig. 10(b) indicate statistically reasonable values. The average field strength obtained by using all of the observation data varies from -127.5 to -129.0 dB with altitude. As the range of variation of 1.5 dB is approximately twice the standard deviation σ_{50} obtained in the process in Fig. 2, this variation seems to be caused by the statistical fluctuation of the background noise. However, the

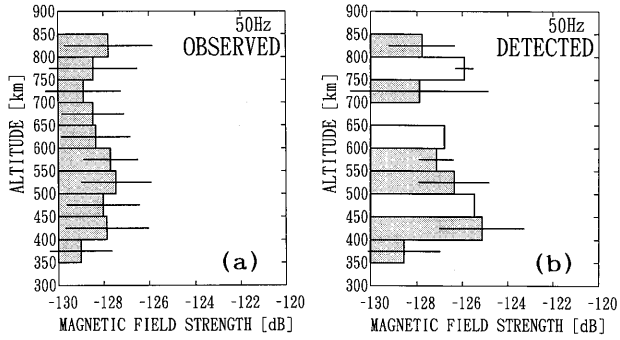

Fig. 10 Average magnetic field strength vs. satellite altitude, (a) for all of the observed data points, and (b) for the detected data points, both for 50 Hz. The horizontal short lines across the top of each bar are the standard deviation of each field strength. Shaded bars in (b) indicate statistically reasonable values.

reasonable average field strength of the detected points varies from -125.1 to -128.5 dB, and the field strength seems to gradually decrease from 400 to 850 km. The low field strength at the lowest bin, 350–400 km, might be caused by the lowest field strength of the background noise at this altitude, as seen in Fig. 10(a).

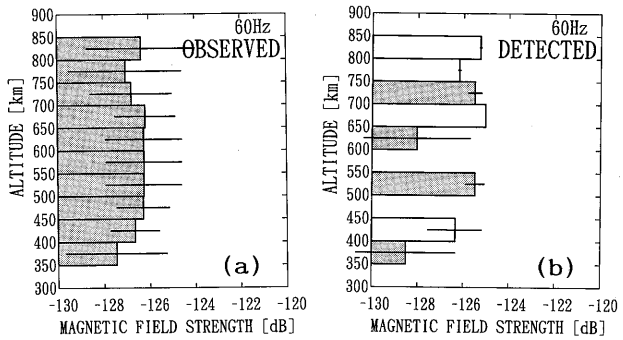

Fig. 11 Average magnetic field strength vs. satellite altitude, (a) for all of the observed data points, and (b) for the detected data points, both for 60 Hz. The horizontal short lines across the top of each bar are the standard deviation of each field strength. Shaded bars in (b) indicate statistically reasonable values.

The altitude dependency of average magnetic field for 60 Hz is shown in Fig. 11(a) for all of the observed data points, and in Fig. 11(b) for the detected data points in the same format as in Fig. 10. The average field strength of all of the observed data varies from -125.5 to -126.2 dB with altitude. As the range of variation of 0.7 dB is approximately the same as the standard deviation σ_{60} obtained in the process in Fig. 2, this variation seems to be caused by the statistical fluctuation of the background noise. Although the average field strength of the detected points varies from -125.0 to -128.5 dB, the reasonable field strength does not show a systematic variation. This difference may be caused by the small number of detected points at 60 Hz since only four bins are shaded as the statistically reasonable data.

5. Discussion

5. 1 Statistical Reliability of Detecting PLR

The old technique for detecting PLR adopted from Paper (10) was simply collecting the data points exceeding the $+1\sigma$ limit since there was no technique to distinguish PLR and the background noise under the low signal-to-noise ratio. Therefore, the detected data points inevitably included data points which were mainly filled with background noise, because the determined statistical parameters mainly reflected the statistical characteristics of the background noise. The ratio of the detected points to all of the data did not exceed 15.85% as we had assumed a Gaussian distribution.

The Gaussian distribution of the background noise is confirmed from the result of the statistical fitting procedure newly employed in this paper. It is interesting to note that the Gaussian amplitude distribution was also obtained for ELF-VLF hisses [12]. This supports our results that the background noise at 50 or 60 Hz is caused by the plasmaspheric ELF hiss [10].

Accordingly the number of detected points should be reduced by strictly limiting the detection, e.g., $+2\sigma$ or $+3\sigma$, in order to increase the statistical reliability for detection. However, we can see the relationship between the detected points and the electric power generation over the eastern part of China even for the simple detection criterion of $+1\sigma$. Thus, we noted in Paper (10) that we could expect clear correlations by increasing the reliability of detection, and that an improved technique to distinguish PLR from the background noise will be needed to increase the reliability of detecting PLR in the satellite observation.

The total number of the observed data points becomes 1361, which is 2.70 times as large as the last analysis in Paper (10); then we can perform an improved determination of the statistical parameters such as spectral inclination and standard deviation. The statistical improvement in estimating these parameters is only 1.64 if we assume a simple Gaussian distribution. However, we can see the skewness of the distribution with respect to the straight line as indicated in Fig. 5. The skewness was not noticed in Paper (10) since the statistical ambiguity of the distribution was relatively high. This skewness could not be distinguished by simply calculating the spectral inclination and the standard deviation using all of the observed data points as indicated in Fig. 3(a). As we described in Sec. 2, we can apply the improved technique to the analysis. We can, therefore, expect the statistical discrimination of PLR from the background noise based on the difference in the deviation from the background noise strength. The effect of this skewness appears as the increase of the spectral inclination and the standard deviation. This effect additionally suppresses the detection of PLR by the simple method since the threshold level of the detection should rise for this case.

We apply this new method of an iterative technique to reduce the influence of PLR on the background noise field, as described in Sect. 2. The statistical parameters of the background noise are estimated with a small bias to the original ones, as shown in Fig. 3(d). The amount of this bias depends on the degree of skewness of the combined distribution. This bias should be small for a largely skewed distribution since the separation between PLR and the background noise can be easily recognized. The lower part of the actual distribution fits the estimated curve as shown by the solid curve in Fig. 5. Therefore, the estimated statistical parameters are interpreted as good estimates in this improved method. Additionally the standard deviations of the two distributions are similar for both frequencies; i.e., 0.87 dB and 0.81 dB for 50 and 60 Hz, respectively. The difference between the two values is only 0.06 dB, which is approximately 7% of the esti-

mated values. This similarity is interpreted as indicating that the statistical characteristics at three frequencies, 50, 55 and 60 Hz, are quite similar. Therefore, the assumption of the wideband Gaussian noise can be satisfied. However, the value of the standard deviation for 50 Hz is somewhat larger than that for 60 Hz. This is explained as indicating that the disturbance of PLR to the estimation of the background noise is stronger for 50 Hz than for 60 Hz, that is, the signal-to-noise ratio at 50 Hz is greater than that at 60 Hz. This is also explained by the fact that the number of detected data points is larger for 50 Hz.

To increase reliability of the statistical detection of PLR, we must take the $+3\sigma$ limit instead of the $+1\sigma$ limit since we must reduce the contamination by the background noise. By applying this detection criterion to the actual observation data, we obtain 45 data points for 50 Hz and 21 for 60 Hz. The statistical error in the detection for the $+3\sigma$ limit is only 0.15%, which corresponds to 2.04 for the total data point number of 1361. Therefore, the possible contamination to these detected numbers is approximately 2. The error rates in the detected data are 4% and 10% for 50 and 60 Hz, respectively. Thus we can estimate the relative error rate for the detection.

5. 2 Cause-and-Effect Test for the Detected Data by Correlating with the Electric Power Generation in Eastern Asia

As we mentioned in Sect. 3, the data points detected by the improved method should correlate with the source of PLR such as totally generated power per year, total length of extended power lines, or instantaneous generating power, in Eastern Asian countries. If there is no relationship among them, the statistically detected data are considered to be spurious. The electric power generation is considered as the cause of PLR and the relationship is the effect. This cause-and-effect test is applied for examining the reliability of the detection. We are going to use the totally generated electric powers as the reference parameters of PLR in Eastern Asian countries, because only this parameter is available from the yearly statistics of the United Nations [13]. Fortunately the distribution of the electric generation frequencies in Eastern Asian countries is divided into two regions [4]. Therefore we could separately correlate for each frequency region, and then we can compare the results to emphasize the correlations.

The correlation process is performed as follows: first, correlate the detection ratios with the ground map of the generating frequency, second, correlate the average field strengths with the total electric power generation per year.

The detected data points for 50 Hz are mainly concentrated in two regions: one around Eastern Japan [4] and another around the east coast of China [6], [14], as shown in Fig. 6(b). Furthermore, high detection ratios greater than 30% are concentrated around Eastern Japan. This can be contrasted with the surrounding region, e.g., over Western Japan, over the Pacific Ocean and over central China, where no or a small amount of electric power at 50 Hz is generated. Unfortunately we cannot correlate the detection ratio over Siberia in USSR since no statistics of electric power generation are available now. Therefore these low detection rates over Siberia cannot be discussed here. The average field strength at 50 Hz is also strengthened over Eastern Japan, as shown in Fig. 6(d). Therefore the high detection ratios are the results of high PLR field over these regions since the average field strength of the background noise does not show weakness over these concentrated regions, as seen in Fig. 6(c). It is concluded that the detected data points of 50 Hz are closely correlated with the electric power generation. Thus the cause-and-effect for the detected data of 50 Hz is clearly confirmed.

The total electric power generation through 1985 in China is 4.1×10^{11} kWh [13], [14], and that in Eastern Japan is 3.0×10^{11} kWh [4], as shown in Fig. 6(e). Although the value for China is higher than that for Japan, it is interesting to note that the average field strength over Japan is higher than that of China. This may be caused by electrical structures of power lines or average densities of power lines in these two countries. It must be an interesting problem in electric engineering to compare the power lines in these two countries.

On the other hand, although the detected data points of 60 Hz are concentrated in a relatively dispersed region, as shown in Fig. 7(b), the correlation to the electric power generation is relatively weak for the detected data of 60 Hz, comparing with those of 50 Hz. However, the concentration is reasonable since the concentrated region covers the regions of the electric power generation for 60 Hz, which is indicated in Fig. 7(e). Furthermore, the detection ratios over the region of no electric power generation at 60 Hz can also be contrasted with the detected regions as seen in Fig. 7(b). The direct correlation with this map is only recognized over Western Japan, where the electric power generation, 3.8×10^{11} kWh, in 1985 [4] is highest for 60 Hz, since the detection ratios become 20% around Western Japan. However, as the average field strength does not show enhancement over Western Japan, the enhanced region is not caused by the statistical fluctuation but by the effect of PLR. Other detected regions could be correlated to South Korea, Taiwan and Philippines if these regions could be shifted horizontally. Therefore, it is concluded that the detected data points of 60 Hz are closely correlated to the electric power generation. Thus the cause-and-effect for the 60 Hz data is also confirmed.

The cause-and-effect tests for both frequencies satisfy the requirement of the detection of PLR. We

can clearly say that the detected data points represent PLR over Eastern Asia. Although the electric power generation in Eastern Japan is approximately the same as that in Western Japan [4], the detection ratios over Western Japan are smaller than those over Eastern Japan. The difference in detections must be caused by the signal-to-noise ratio at the satellite altitude, since the electrical structures of power lines in these regions are quite similar, the total electric power generations are almost the same, and the propagation of these frequencies is also similar.

5. 3 Propagation of PLR into the Ionosphere

The magnetic field strength at 50 Hz of the statistically reasonable data gradually decreases with increasing altitude, as shown in Fig. 10. The decreasing rate is approximately 3 dB from 400 to 700 km altitude. The amount of the decrease, 3 dB, exceeds the statistical ambiguity of the reasonable data of 2 dB as indicated by the error bars as shown in Fig. 10(b). Therefore, this decrease is not caused by the statistical fluctuation of the reasonable data. Radio waves at 50 or 60 Hz propagate in the whistler mode [1] from 400 to 700 km altitude, when the ionospheric ion and electron densities are provided by the CIRA-1972 [3] and IRI79 [8] models in Eastern Asia. The magnetic field strength of the whistler mode wave is proportional to the square root of the real part of the refractive index [2] when the attenuation can be ignored and the electron and ion densities show gradual variations with altitude. The ratio of the real part of the refractive index at 400 km to that at 700 km is approximately 3 for the assumed ionospheric model; therefore, the ratio of the magnetic field strength at these altitudes is approximately 5 dB. Although the calculated ratio of 5 dB is 2 dB greater than the observed ratio of 3 dB for 50 Hz, this can be explained by the statistical ambiguity of the observation. On the other hand, the background noise at 50 Hz does not show a gradual decrease with increasing altitude but only indicates a small enhancement at about 500 km, as shown in Fig. 10(a). If the background noise propagates as the whistler mode wave upward from the bottom of the ionosphere, a comparable amount of attenuation should be observed on the background noise. It can be explained that the background noise is propagating downward from the top of the ionosphere. However, if it propagates in the whistler mode, it should also indicate the same amount of decrease with altitude. Therefore it is necessary to decrease the field strength at the lower altitude. The whistler mode wave propagating downward must be reflected at the bottom of the ionosphere. Thus, the decrease of field strength at the lower altitude can be interpreted as the interference effect of the down-going and up-going waves. This speculation of the altitude dependencies should be examined by a quantitative calculation.

The magnetic field strength of the detected data at 50 Hz shows gradual decrease with increasing altitude while that of the background is almost constant from 400 to 700 km altitude. Therefore, the altitude dependency of the detection ratio is explained by the decrease of signal-to-noise ratio when the PLR field is propagating upward under the approximately constant field strength of the background noise by decreasing the field strength with increasing altitude.

According to the result of Sect. 4.2 on the cause-and-effect test, the detected data points are concentrated into relatively small regions around the high electric power generating regions, such as Eastern Japan, the east coast of China and Western Japan. As the high contrast of the PLR field is found in this analysis over Eastern Asia, the propagation of PLR from the source region, where power lines are extended, to the satellite altitude does propagate in the narrow range of direction. However, the detected regions seem to expand toward the south or southeast of Eastern Japan, toward the southeast of China, and toward the south of Western Japan. Therefore we can infer the horizontal map of PLR under the ionosphere if we can estimate the propagation into the ionosphere.

The relationship between the distribution of electric power generation and the detected region for 60 Hz is revealed only for Western Japan in this analysis. Although it is possible to infer relations of the scattered region of 60 Hz by shifting some extent, the explanation does not indicate systematic shifts for these regions. Therefore, more observation data are required to examine the relationships for 60 Hz.

According to the results of the calculation for the penetration of incident waves at the VLF range [7], the contour map of the intensity of the whistler mode wave penetrating into the ionosphere shows a small and high-intensity region and a southward deviation of its location for the northern hemisphere. The wave at 50 or 60 Hz can also penetrate into the ionosphere as the whistler mode wave [1]. Then the whistler mode wave tends to align the geomagnetic field line. As the direction of the geomagnetic field lines around Japan is almost in the meridian plane, the PLR wave may propagate to the southward direction. The deviation toward south or southeast can be explained by the lateral shift of the contour map with respect to the distribution of the electric power generation on the ground map. Therefore, the detected data points extend southward for Eastern Japan and Western Japan, as shown in Figs. 10(b) and 11(b). These deviations must be explained by the quantitative calculation.

6. Conclusions

The data used in this analysis were obtained by the

observations of the scientific satellite OHZORA from June 1984 to January 1986. The total number of orbits is 150, which is five times as large as that in our last paper [10]. This observation covers Eastern Asian countries including Japan, China, South Korea, North Korea, Taiwan, Philippines and USSR, where two power generating frequencies are used and power generation is relatively concentrated in small regions. Based on the increase in the number of data points to 1361, the statistical characteristics of the background noise are precisely determined by using the improved technique compared with the initial analysis [10]. Statistically reasonable data points are detected as PLR based on the $+3\sigma$ criterion, where σ is the standard deviation of the background noise. By applying this detection technique to the actual observation data, we obtain 45 data points for 50 Hz and 21 for 60 Hz. The statistical error in the detection for the $+3\sigma$ limit is only 0.15%, which corresponds to 2.04 for the total data of 1361. Therefore, the error rates to the detected data are 4% and 10% for 50 and 60 Hz, respectively. Thus we can conclude that the statistical reliability of the PLR detection is 99.85%, according to the rejection rate of the background noise. However, the detection process is only dependent on the statistical meaning. Therefore, it is necessary to examine whether these detected data points are actually correlated to the possible PLR on the ground. As the cause-and-effect tests for both frequencies satisfy the requirement of the detection of PLR, it is concluded that the detected data points are closely related to the electric power generation in Eastern Japan and the east coast of China for 50 Hz, and in Western Japan for 60 Hz. Therefore, we can clearly say that the detected data points represent PLR over Eastern Asia.

The detection ratio and the average magnetic field strength over Eastern Japan are higher than those over China while the total electric generation power in China is 1.4 times as large as that in Japan. The difference can be explained by the difference in the densities or in the electrical structures of power lines in these countries. It is necessary to examine which parameter is effective in the observed difference.

Although the electric power generation in Western Japan is 1.3 times as large as that in Eastern Japan, the detection ratios over Western Japan are smaller than those over Eastern Japan. The difference in the detection ratio must be caused by the signal-to-noise ratio at the satellite altitude, since the structure of power lines in these regions is the same, the total electric power generation is almost the same, and the propagation of these frequencies is also similar.

The decrease of field strength with altitude is interpreted as the gradual decrease of the refractive index from 400 to 700 km. On the contrary, as the background noise does not indicate such a decrease with altitude, it propagates not from the bottom but from the top of the ionosphere. Therefore, the altitude dependency of the detection ratio is explained by the decrease of signal-to-noise ratio when the PLR field is propagating upward under the approximately constant field strength of the background noise by decreasing the field strength with increasing altitude. We conclude for the propagation characteristics of 50 and 60 Hz as follows: 1) The penetration of PLR into the ionosphere is just over or close to the source region where power lines are extended. 2) The propagation in the ionosphere does not greatly deviate from the source regions but is somewhat expanded toward the south or southeast. 3) The magnetic field in the ionosphere is gradually decreased by the rate of 3 dB from 400 to 700 km. Further explanation of these propagation characteristics will be presented in another paper.

As the generation of the electric power in Eastern Asia doubles in 10 years [13], the electromagnetic field should also increase at a similar rate since the power transmission line system may not be changed throughout this period. Therefore, the increase of electric power generation in 10 years will give us a 3 dB increase in the magnetic field strength above power lines. So we can predict the increase of PLR field strengths at the satellite altitude at this rate. Thus the electromagnetic field of PLR in the ionosphere or in the magnetosphere may exceed the background noise fields and then may become an interference source at the ELF range in the future.

We have clearly shown the distributions of the magnetic field strength over Eastern Asia in this paper based on satellite observation. Further observation and calculation are required to draw the corresponding distribution just over power lines in order to estimate the radiation model of PLR.

Acknowledgement

We are greatly indebted to Prof. T. Itoh of the Institute of Space and Astronautical Science (ISAS), Prof. H. Oya of Tohoku University, and Prof. Y. Nakamura of ISAS, for the satellite research project of "OHZORA." We thank Prof. M. Hayakawa of the Univ. of Electro-Comm. for his helpful comments, and Mr. K. Asami for processing a large amount of data.

References

[1] Booker, H. and Lefeuvre, F., "The relation between ionospheric profiles and ELF propagation in the Earth-ionosphere transmission line," *J. Atmos. Terr. Phys.*, vol. 39, pp. 1277-1292, 1977.
[2] Budden, K.G., *The Propagation of Radio Waves,* Cambridge Univ. Press, Cambridge, 1985.
[3] COSPAR, *CIRA 1972,* Akademie-Verlag, Berlin, 1972.
[4] Denki-Jigyo-Rengoukai-Toukei-I-Inkai, *Denki-Jigyou-Binran,* Syouwa-61nen-Ban, Nihon-Denki-Kyoukai,

Tokyo, 1986.

[5] Galejs, J, *Terrestrial Propagation of Long Electromagnetic Waves,* Pergamon Press, Oxford, 1972.

[6] Miura, M., "Electric power generation in China," *OHM*, vol. 76, pp. 65-70, 1989.

[7] Nagano, I, Kitagishi, Y., Yagitani, S., Mambo, M. and Kimura, I., "Mapping of VLF intensities in the ionosphere by a dipole antenna on the ground," *Trans. IEICE,* vol.J74-B-II, no. 5, pp. 285-293, 1991.

[8] Rawer, K., "International Reference Ionosphere-IRI79," Report UAG-82, World Data Center A for Solar-Terrestrial Physics, NOAA, Boulder, Co., U.S.A., 1981.

[9] Tomizawa, I. and Yoshino, T., "Distribution of horizontal magnetic field induced and radiated from power lines," *Bull. Inst. Space Aeronaut. Sci., Univ. Tokyo,* vol. 16, no. 2(B), pp. 1123-1132, 1980.

[10] Tomizawa, I. and Yoshino, T., "Power Line Radiation Observed by the Satellite OHZORA," *J. Geomag. Geoelectr.,* vol. 37, pp. 309-327, 1985.

[11] Tomizawa, I., "Estimation method of mechanisms of power line radiation by using balloon observations," *IEICE Technical Report,* EMCJ90-91, 1991.

[12] Tsuji, S., Hayakawa, M., Shimakura, S. and Hattori, K., "On the statistical properties of magnetospheric ELF/VLF hiss," *Proc. NIPR Symp. Upper Atmos. Phys.,* vol. 2, pp. 74-83, 1989.

[13] United Nations, *World Energy Statistics Yearbook (1987),* United Nations, New York, 1987.

[14] Xi, X.-L. and Morgan, M. G., "Energizing China: first itself, next the world," *IEEE Spectrum,* vol. 26, pp. 59-63, 1989.

[15] Yoshino, T. and Tomizawa, I., "Rocket and balloon observations of power line radiation over Japanese Islands," in *Proc. 4th EMC Meeting, Zurich,* pp. 525-530, 1981.

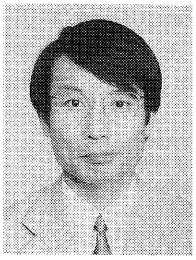

Ichiro Tomizama received his B.E. and M.E. degrees from the University of Electro-Communications (U.E.C.) in 1975 and 1977, respectively. In 1977 he joined Sugadaira Space Radio Observatory, U.E.C., in Nagano, Japan as a research associate, where he was engaged in the investigation of Jupiter's Decametric Emissions from 1977 to 1984, and in the satellite tracking and receiving system from 1980 to 1988. He has started the research on power line radiation in 1978. In 1990 he moved to the Department of Electronic Engineering, U.E.C., in Tokyo, Japan. His current research interest is in electromagnetic compatibility including power line radiation and the electromagnetic phenomena associated with crustal deformations. He is a member of the Society of Geomagnetism and Earth, Planetary and Space Sciences, the Astronomical Society of Japan, and American Geophysical Union.

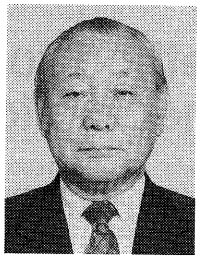

Takeo Yoshino received his B.E. degree in 1953 from the University of Electro-Communications, Tokyo, Japan. In 1953, he joined the Department of Electronic Engineering of the University of Electro-Communications. Since 1973 he has been a Professor in the same Department, and since 1970 he has been the Director of Sugadaira Space Radio Observatory of the same University. From 1958 to 1960, he stayed at Syowa Station in Antarctica as a wintering party member of the third Japanese Antarctic Research Expedition, and from 1975 to 1977, he was at Syowa Station again as the leader of the 17th Expedition. In Antarctica, his main field of interest was the analysis and investigation of the auroral phenomena by the natural VLF radio wave emissions observed by rockets and satellites. Today his research interests are the emission mechanism of electrostatic ion-cyclotron waves and VLF auroral hiss over auroral oval by satellite observations, the prediction of earthquakes and volcano eruptions by means of the seismogenic emission phenomena, the bio-effects of radio emission and VDT in EMC fields, and the observation and development of the burst VLBI system in millimeter-band radio astronomy. He received the IEEE-AP Best Paper Award in 1967, and a Distinguished Service Award on EMC from the Polish EMC Symposium in 1992. Prof. Yoshino is a member of IEICE and EPEMJ (Japan), IEEE and AGU (USA), URSI, IAGA and COSPAR, an advisory board member of Zurich EMC Symposium, Wraclow EMC Symposium, and Lowell Observatory, and the chairman of IEEE-EMCS Tokyo chapter.